Measuring and Extraction of Biological Information on New Handheld Biochip-Based Microsystem

Paulo A. C. Lopes, José Germano, Teresa Mendes de Almeida, Leonel Augusto Sousa, *Senior Member, IEEE*, Moisés S. Piedade, Filipe Arroyo Cardoso, H. A. Ferreira, and Paulo P. Freitas

***Abstract*—This paper proposes techniques for the extraction of biological information in a recently developed handheld biochip-based microsystem. The microsystem is based on a magnetoresistive array biochip composed of a number of sensing sites with magnetic tunneling junctions (MTJ) and diodes. Different techniques are addressed to drive the MTJs with different types of signals. Different filtering strategies that allow the recovery of biological signals from the noise without overly increasing either the time required for accessing the sensors or the power consumption of the board are proposed. Finally, new techniques and algorithms are proposed to deal with the variability of the fabrication parameters of the MTJ and the diodes. Experiments with the system in a setup to detect actual biological signals are presented with encouraging results.**

***Index Terms*—Biochip, biomolecules, magnetic sensors, microsystem, signal processing.**

I. Introduction

ONE of the trends of the last decade has been the miniaturization of typical large laboratory experiments. This has been made possible by the advance in microfluids and microelectromechanical systems (MEMS) technologies. One of the outcomes of this trend has been the so-called "lab-on-a-chip" system [1]. For lower scale production, microsystems such as that described in this paper offer great promise.

We developed the microsystem used in this paper, which is based on magnetoresistive biochips [2]. These chips have been introduced for fully integrated biomolecular recognition assays [3], [4]. In these experiments, target biomolecules are marked with magnetic particles and are subsequently recognized by biomolecular probes immobilized at the surface of the chip over sensing sites. The marked magnetic fringe fields are then detected by magnetic tunneling junctions (MTJs) [1].

The developed system consists of a compact credit-card-dimension portable handheld microsystem for biomolecular recognition assays. The microsystem includes the magnetoresistive biochip and all the electronics that are necessary to address and read the sensors and to implement temperature and fluid control. This paper mainly addresses the signal processing techniques and algorithms for measuring and extracting biological information on this new handheld microsystem.

Manuscript received November 14, 2007; revised June 19, 2008. First published October 14, 2008; current version published December 9, 2009.

P. A. C. Lopes, T. M. de Almeida, and L. A. Sousa are with Instituto Superior Técnico, Technical University of Lisbon, 1049-001 Lisbon, Portugal, and also with the Instituto de Engenharia de Sistemas e Computadores-Investigação e Desenvolvimento (INESC-ID), 1000-02 Lisbon, Portugal (e-mail: paulo.c.lopes@inesc-id.pt).

J. Germano is with Instituto Superior Técnico, Technical University of Lisbon, 1049-001 Lisbon, Portugal.

M. S. Piedade is with Instituto de Engenharia de Sistemas e Computadores-Investigação e Desenvolvimento (INESC-ID), 1000-02 Lisbon, Portugal.

F. A. Cardoso and H. A. Ferreira are with Instituto de Engenharia de Sistemas e Computadores Microsistemas & Nanotecnologias (INESC-MN), 1000-029 Lisbon, Portugal (e-mail: fcardoso@inesc-mn.pt)

P. P. Freitas is with Instituto Superior Técnico, Technical University of Lisbon, 1049-001 Lisbon, Portugal, and also with Instituto de Engenharia de Sistemas e Computadores Microsistemas & Nanotecnologias (INESC-MN), 1000-029 Lisbon, Portugal.

Color versions of one or more of the figures in this paper are available online at http://ieeexplore.ieee.org.

Digital Object Identifier 10.1109/TIM.2008.2003321

II. Architecture

The proposed architecture for the biochip platform is organized into two main modules (Fig. 1): 1) the sensing and processing module (SPM) and 2) the fluid control and communication module, as represented in Fig. 1.

A. Reading and Controlling Circuits

The core of the system is the 16-bit integrated microcontroller/digital signal processor (MC/DSP) Microchip dsPIC 30F6014. This device has a performance of up to 30 MIPS and an extended instruction set for digital signal processing. A static random-access memory (RAM) is also included. This MC/DSP addresses and reads the data from the array of magnetoresistive sensors provided by the biochip and measures and controls the temperature by using those same devices.

1) Current Generator Circuits: To perform readings in the complete sensor array, the current to the sensor is generated using a digital-to-analog converter (DAC) and a voltage-to-current converter and is multiplexed into the biochip. Fig. 2 depicts the circuit diagram employed in the current generator. In this circuit, the current that flows to the sensor is the same current that runs through R_F, which is defined by $i_M = v_{\mathrm{DAC}}/R_F$. This decreases the temperature and the current errors introduced by the current mirror that drives the sensor and by transistor Q_F.

For the required external magnetic field generator, a circuit similar to that used for the generation of the sensor driving current is used. The current intensity in the coil (ac and dc) and, consequently, the magnetic field is controlled using the DAC and scaled through a resistor.

2) Heater/Carrier: The heater/carrier line represented in Fig. 1 is designed with a U-shaped geometry around each

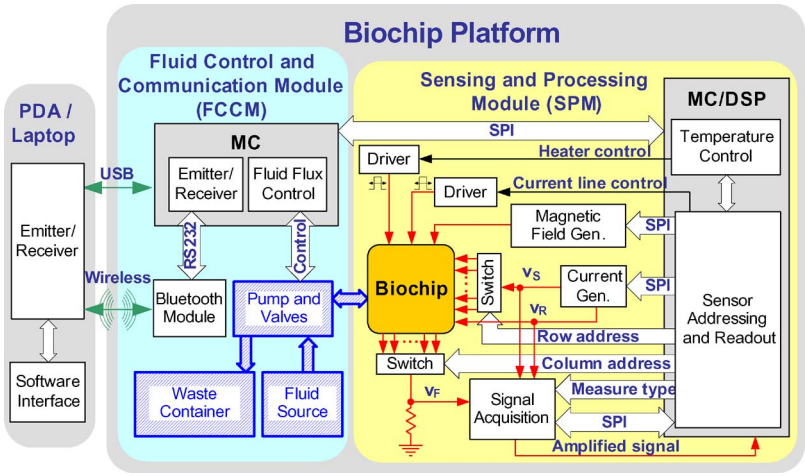

Fig. 1. Full diagram of the microsystem.

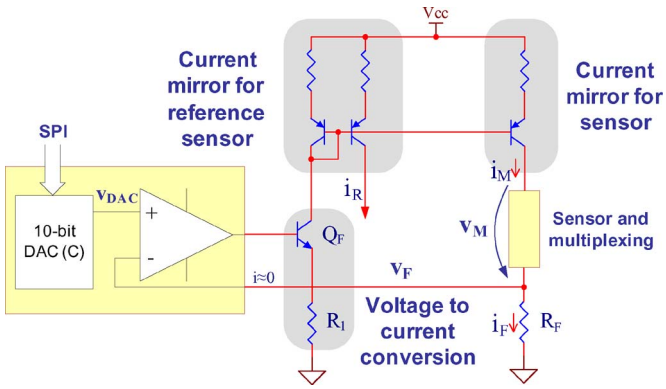

Fig. 2. Current generation circuit.

Fig. 3. Prototype microsystem main board (SPM).

magnetic sensor. By applying a low-frequency current (∼0.1 Hz), the magnetically labeled biological targets are carried to the top of each sensing site [5].

3) Prototype: The prototype of the SPM is shown in Fig. 3. The biosensor array can be seen at the top of the figure, and the MC/DSP and the 1-Mb RAM chip can be seen at the bottom.

III. Biochip Sensing Site

The biochip was fabricated using state-of-the-art, thin-film microelectronic techniques in the Instituto de Engenharia de Sistemas e Computadores Microsistemas & Nanotecnologias

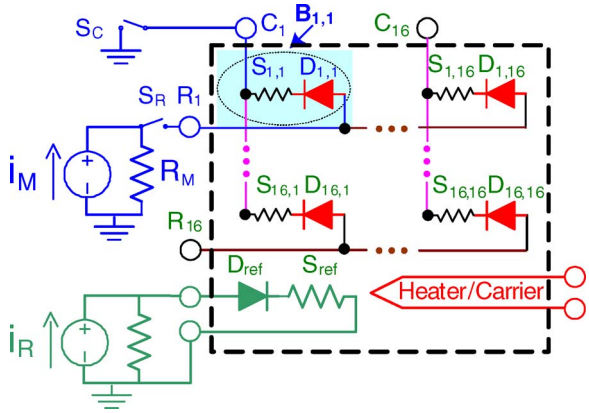

Fig. 4. Magnetoresistive biochip schematic (inside the dashed line).

[6]. The schematic diagram of the biochip is shown in Fig. 4. It is composed of a number of sensing sites formed by an MTJ and a junction diode. The sites are arranged in an array (16×16) and are accessed through line and column wires that are selected through multiplexers outside the chip. The diode has two functions: 1) as a commutator that prevents sites, other than the selected site, from being accessed and 2) as a temperature sensor for biological reactions that take place on each chip site. A typical set of magnetic tunnel junctions used in the biochip was characterized in [7]. The resistance of the MTJ varies with the transversal component of the applied magnetic field. An important characteristic of the junction is its tunneling magnetoresistance ratio (TMR), which is given by

$$\text{TMR} = \frac{R_{\max} - R_{\min}}{R_{\min}} \tag{1}$$

where $R_{\max}$ and $R_{\min}$ are the maximum and minimum resistance values obtained with magnetic opposite saturation fields, respectively. The resistance variation follows a hysteresis curve. Assuming that the junction is being driven by a current I_0, the sensitivity to the magnetic field of the measured voltage signal is given by

$$\frac{\partial v}{\partial h} = S_H^v = \text{TMR(V)} \frac{R_J}{\Delta H_{\max}} I_0. \tag{2}$$

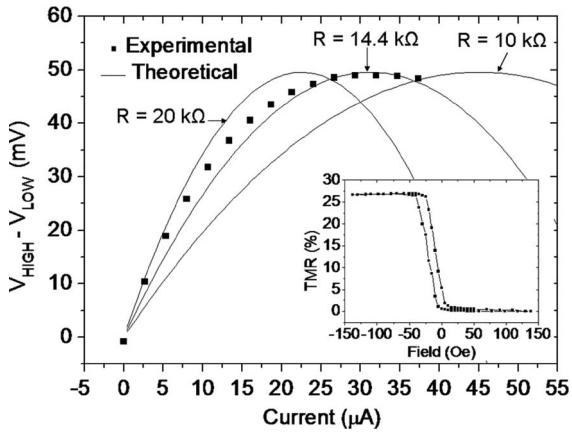

Fig. 5. Variation of the MTJ signal voltage with the applied current.

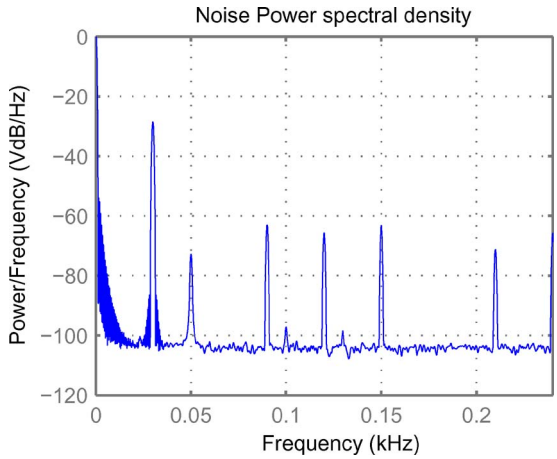

Fig. 6. Input noise power spectral density after the ADC with the DAC configured to a maximum current of 1 mA.

The TMR almost linearly decreases with applied voltage within a range up to 500 mV. It is maximum with zero applied voltage TMR(0). This can be modeled as

$$\frac{\text{TMR(V)}}{\text{TMR}(0)} = 1 - \frac{V}{2V_{1/2}} \tag{3}$$

where $V_{1/2}$ is about 350 mV [7]. This suggests the use of low junction polarization voltages. However, a low polarization voltage implies a low driving current.[1] The sensitivity to the magnetic field of the measured voltage signal, which is given by (2), is optimal for the driving current of

$$I_0 = \frac{V_{1/2}}{R_J}. \tag{4}$$

For the junction in [7], which has about 14.4 kΩ, the optimum current is at about 30 μA, as shown in Fig. 5.

IV. Signal Acquisition: Driving and Sensing

To measure the resistance of the MTJ, a known current was applied at each biosensor, and the resulting voltage was measured. Some important design considerations are discussed in the succeeding sections.

A. AC and DC Measures

Applying a current through the sensing site and measuring the voltage signal will result in a signal that combines the voltage drop across the diode and across the MTJ. To extract the diode signal, one can simply subtract the signal measured before the insertion of the particle solution at the sensor. The result is a signal that is proportional to the number of particles immobilized over the MTJ.

However, this signal is a small signal that is embedded in a large signal. A typical value for this may be about 100 μV. Even with a fully saturated MTJ, the signal level will be about 50 mV. This signal level requires the analog-to-digital converter (ADC) to have a large dynamic range. This problem can be reduced if the applied external magnetic field has a sinusoidal component. This alternating magnetic field will produce a corresponding variation on the MTJ resistance value. This signal can then be separated from the dc bias voltage through a high-pass filter and then amplified.

B. Selecting the Drive Current Value

Note that, in Fig. 5, the driving current was optimized for the highest signal level. If the requirements were to optimize the signal-to-noise ratio, then the results would be different. However, for this application, as we will see later, the noise level is not limited by the junction.

V. System Noise Performance

The magnetic particle detection of the system is limited by its noise performance and measuring resolution. Each biosensor contributes 1/f noise with a spectral density of about 370 nV/$\sqrt{\text{Hz}}$ at a measuring frequency of 300 Hz and about 3.7 μV/$\sqrt{\text{Hz}}$ at 30 Hz when fed with an optimal reading current of 30 μA. However, the overall system has a higher equivalent input noise voltage, as we will see next. Measurements of noise levels in the board were made for the case of a sinusoidal current drive signal (ac mode). The sampling frequency is 480 Hz. The signal is a 30-Hz, 5-μA current injected through a 10-kΩ resistance. The noise power spectral density is shown in Fig. 6. The noise is mostly composed of five components: 1) harmonics of the 30-Hz frequency; 2) quantization noise from the DAC; 3) 50-Hz power line frequency noise; 4) low-frequency noise; and 5) white noise. The total noise level reaches 1 mV_{RMS}, due to DAC quantization. The 50-Hz power line noise and low-frequency noise amount to 370 μV_{RMS}, and the resulting noise is about 37 μV_{RMS}. Further filtering with a 3.3-s-length bandpass filter (a finite impulse response (FIR) filter with 1584 taps) reduces the noise to about 8 μV_{RMS}.

[1]Note that, due to the ultralow thickness of the dielectric, the MTJ may break down for applied voltages over 1.1 V. For example, for MTJs with $R_J = 15.3$ kΩ, the maximum drive secure driving current is 65 μA.

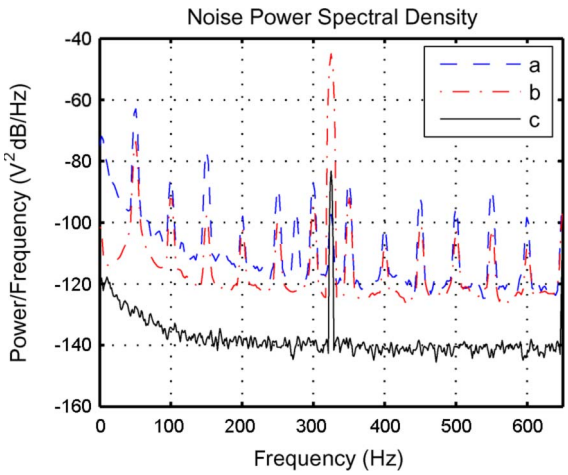

Fig. 7. Noise power spectral density relative to the sensing site measured by the ADC with the DAC configured to a maximum current of 100 μA and the board set to ac mode. In lines a and b, the system has a gain of 10. In line a, the load is a sensing diode site. In line c, the board is shielded, and the gain is 899. The peak at 325 Hz is the applied signal.

The quantization noise leads to a change of the DAC scale from a maximum of 1 mA to only 100 μA. The change of the board to ac mode with a gain of 10 leads to the reduction of the noise floor by ten to 1 $\mu\text{V}/\sqrt{\text{Hz}}$, as shown in Fig. 7 (line b). The noise level when the load is set to a sensing site diode is shown in Fig. 7 (line a), where a high low-frequency noise is visible, which leads to an increase in the signal frequency to 325 Hz, with a sample ratio of 4 spl/period and a conversion ratio of 1300 cvs/s. In Fig. 7 (lines a and b), there is a strong 50-Hz interference signal. This can easily be removed through digital processing, but it limits the gain of the amplifier. In Fig. 7 (line c), the board was shielded using an iron and Mu-metal case, removing the 50-Hz signal and allowing the gain to be increased to 899. This resulted in further reduction of the noise floor to about 100 $\text{nV}/\sqrt{\text{Hz}}$.

VI. Signal Processing

In the system, there are two main tasks for the signal processor embedded in the board: 1) the generation of the drive signal and 2) the recovery of the biological signal. Some of the signal processing techniques rely on previously obtained models for the MTJ and diode [7].

A. Generating the Drive Signal

For ac measurements, a sinusoidal driving signal was chosen, while for dc, a constant current was used. The sampling ratio was chosen to be a constant multiple of the sinusoidal signal. This allows the signal to be generated by the DSP in a very simple way through a lookup table.

The output of the DAC resembles a staircaselike signal, due to the sample-and-hold, which could be interpreted as nonlinear distortion of the sinusoidal signal. However, since the ADC samples this signal at the same frequency, this is not the case. In fact, the action of the sample-and-hold can be integrated with the frequency response of the system in a linear way so that the full loop from the DAC to the ADC can be viewed as a discrete-time linear system, as shown in

$$s_{\text{ad}}(t) = \sum_n y[n]\delta(t - nT_a) * h(t). \tag{5}$$

The only nonlinear distortions that do occur are due to quantization caused by the limited resolution of the DAC (10 bits). Taking this into account, it is safe to say that there is no need for the inclusion of a reconstruction filter at the DAC output. However, a filter at the ADC input is desirable to reduce the noise acquired by the ADC, which can be, for example, the antialiasing filter.

B. Noise Filtering

Assuming an ac drive, either with an ac magnetic field or an ac current through the sensor, the amplitude of the voltage signal at the sensing site must be determined. This can be done using several techniques. The measured signal $y[n]$ can be approximated by the sinusoidal signal, with analog frequency f_0, which corresponds to the digital frequency $w_0 = 2\pi f_0/f_s$ ($f_s \equiv$ sample frequency). The signal is corrupted by white noise $v[n]$ with standard deviation σ_v

$$y[n] = A\cos(\omega_0 n + \phi) + v[n] \tag{6}$$

and the goal is to estimate the amplitude A of the signal. Three techniques are proposed. The discrete Fourier transform (DFT) amplitude estimator in Section VI-B2 was chosen for implementation. The method in Section VI-B3 is optimal but can be reduced to that in Section VI-B2. It corresponds to a matched filer [8] that maximizes the output signal-to-noise ratio. In [9], methods are addressed to estimate complex sinusoid amplitudes in white and colored noise, and our methods are related to the least-squares (LS) estimator. In [10], Rife and Boorstyn show the maximum-likelihood estimator for the unknown phase, which is presented in Section VI-B2.

1) RMS Value Calculation: One approach is to calculate the RMS value of the received signal, as given by (7). This only gives reasonable results as long as the noise level is low. If this is not the case, the signal can first be bandpass filtered to reduce the noise, although this can be more costly than the operations in other methods. Assuming that N samples are taken from the received signal, where N is a multiple of the signal period, then the signal amplitude estimate will be

$$A_{\text{RMS}} = \sqrt{\frac{2}{N}\sum_{n=n_0}^{n_0+N-1} y[n]^2}. \tag{7}$$

This amplitude estimator is biased, its expected value is given by

$$E[A_{\text{RMS}}/A] = 1 + (\sigma_v/A)^2 \tag{8}$$

and the standard deviation or RMS value of the noise will be $\sigma_{(A_{\text{RMS}}/A)} = \sqrt{(2/N)}\sigma_{(v/A)}$.

2) DFT Amplitude Estimator: Since we intend to calculate the amplitude of the received signal, an obvious approach is to calculate its DFT and determine the amplitude at the drive frequency. However, it is not required to calculate the full DFT: only its amplitude at the given frequency. This can be calculated by

$$I = \frac{\sum_{n=n_0}^{n_0+N-1} 2y[n]\cos(\omega_0 n)}{N} \tag{9}$$

$$Q = \frac{\sum_{n=n_0}^{n_0+N-1} 2y[n]\sin(\omega_0 n)}{N} \tag{10}$$

$$A_{\mathrm{DFT}} = \sqrt{I^2+Q^2}. \tag{11}$$

This is an unbiased estimator of the amplitude. Its standard deviation, for small values of the noise signal, is given by

$$\sigma_{(A_{\mathrm{DFT}}/A)} = \sqrt{\frac{2}{N}}\sigma_{(v/a)}. \tag{12}$$

This result is the same as that from the RMS calculation. However, since this estimator is almost unbiased, the resulting estimation error is usually much lower. This technique can also be interpreted as the use of two bandpass filters, which measure the in-phase (I) and quadrature (Q) signal components. If one wishes to filter out higher harmonics from the signal, which may not be precisely controlled, then N should be chosen to be a multiple of the period. The square-root operation can be costly to implement but would not limit the sampling rate of the system.

3) Optimal Passband Filter: Assuming a model for the noise signal in (6), namely, its power spectral density or its autocorrelation function, an optimal filter for removing the noise can be determined in the form of an FIR filter with impulse response w_j and length N [11]. We chose an FIR filter because of the limited time window to the signal at each sensor, which can easily be implemented with FIR filters.

This can be formulated as a Winner filtering problem [12], where $d[n] = A\cos(\omega_0 n + \phi)$ in (6) is the desired signal, and $y[n]$ is the input signal. The input $y[n]$ can be decomposed in two components: $y_0[n] = A\cos(\omega_0 n + \phi)$ and $v[n]$. Only $v[n]$ is considered to be stochastic. If one assumes that the noise is white, as is approximately the case around the drive frequency (Section V), then the optimum filter results in the truncation of a sinusoidal signal. Defining $\mathbf{y}_0 = [y_0[n], \ldots, y_0[n-N+1]]^T$ and $\mathbf{w} = [w_0, \ldots, w_{N-1}]^T$, the autocorrelation matrix of the signal is given by $\mathbf{R}[\mathbf{n}] = \mathbf{y_0}\mathbf{y_0}^T + \sigma_v^2\delta[i-j]$, and the cross-correlation vector is $\mathbf{P}[n] = \mathbf{y_0}y_0$. This will result in a time-varying optimal filter $W[n]$. The output of this filter is then sampled at its maximum to determine the amplitude of the sinusoid, resulting in

$$\mathbf{w} = \frac{\mathbf{y_0}y_0[n_{\max}]}{\mathbf{y_0}^T\mathbf{y_0} + \sigma_v^2}. \tag{13}$$

For the given $\mathbf{y}_0$, as long as σ_v^2 is low and N is a multiple of the period, this reduces to $w_j = 2\cos(\omega_0 j + \phi)$, which, in fact, corresponds to the calculation of the correlation of the received signal with the drive signal. The resulting estimator is then

$$A_{\mathrm{Opt}} = \frac{\sum_{n=n_0}^{n_0+N-1} 2y[n]\cos(\omega_0 n + \phi)}{N}. \tag{14}$$

This is also an unbiased estimator, and the standard deviation is the same as that for the DFT amplitude estimator (Section VI-B2). However, this technique requires the knowledge of the phase of the measured signal. If $\cos(\phi)$ and $\sin(\phi)$ are calculated from $I/\sqrt{(I^2+Q^2)}$ and $Q/\sqrt{(I^2+Q^2)}$, then the method in Section VI-B2 is obtained.

The filter obtained corresponds to the truncation of a sinusoidal signal. It matches the design of a single-frequency extraction filter using the rectangular window method [11]. This method is optimum in the presence of white noise, as in our case. Other methods of filter design, i.e., minimax methods, lead to elliptic filters for infinite impulse response or equiripple filters for FIR. These methods are optimum in the minimax sense, so that any signal in the stop band is attenuated at least A dB but are no longer optimum when the noise spectrum is known.

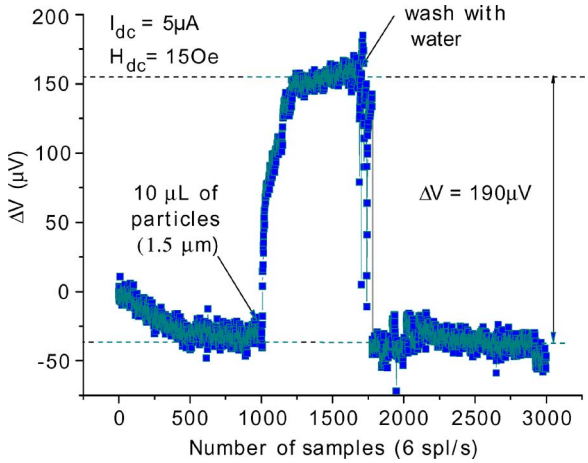

Fig. 8. Time variation of the measured signal for evaluation of particle detection capabilities.

VII. Experiment

The microsystem was tested using a solution of 2.3×10^9 particle/mL with 1.5-μm-diameter magnetic nanoparticles. An 5-μA dc current was driven by the DAC through a 10-kΩ MTJ. The voltage signal was measured by an ADC at a sample rate of 6 Hz after passing through a suitable antialiasing filter. The measurement time was about 8 min. The measured signal is shown in Fig. 8, after the removal of a 47-mV dc signal. The solution was dropped on the sensor after about 1000 samples, and the sensor was washed with distilled water after about 1750 samples. The figure clearly shows a 190-μV signal due to the presence of magnetic particles, demonstrating that the microsystem can be used for particle detection. In addition, if the current level was increased to 50 μA, the signal level could be increased to 300 μV, but this would lead to higher noise levels and lower the signal-to-noise ratio.

VIII. Conclusion

New techniques and algorithms are proposed to measure and extract biological information in a recently developed handheld biochip-based microsystem. A noise floor of 100 $\text{nV}\sqrt{\text{Hz}}$ has been reached. Different filtering strategies, based on the analysis of the noise levels in the system, are also proposed. These strategies allowed the noise to be filtered without excessively increasing the total time required to measure the signals at the sensors while maintaining a low computational complexity and power consumption of the board. The proposed techniques are fundamental to measure and extract biological information. Moreover, experimental results show accurate results when applied to real biological signal detection.

References

[1] D. M. W. Shen, X. Liu, and G. Xiao, "In situ detection of single micron-sized magnetic beads using magnetic tunnel junction sensors," *Appl. Phys. Lett.*, vol. 86, no. 25, p. 253 901, Jun. 2005.

[2] M. Piedade, L. Sousa, J. Germano, J. Lemos, B. Costa, P. Freitas, H. Ferreira, F. A. Cardoso, and D. Vidal, "Architecture of a portable system based on a biochip for DNA recognition," in *Proc. XX Conf. Des. Circuits Integr. Syst.*, 2005. CD-ROM.

[3] M. Johnson, *Magnetoelectronics*. New York: Academic, 2004, ch. 7, pp. 274–331.

[4] A. F. Hugo, D. L. Graham, and P. P. Freitas, "Magnetoresistive-based biosensors and biochips," *Trends Biotechnol.*, vol. 22, no. 9, pp. 455–462, Sep. 2004.

[5] H. A. Ferreira, N. Feliciano, D. L. Graham, L. A. Clarke, M. D. Amaral, and P. P. Freitas, "Rapid DNA hybridization based on ac field focusing of magnetically labeled target DNA," *Appl. Phys. Lett.*, vol. 87, no. 1, p. 013 901, Jul. 2005.

[6] F. A. Cardoso, H. A. Ferreira, J. P. Conde, V. Chu, P. P. Freitas, D. Vida, J. Germano, L. Sousa, M. S. Piedade, B. A. Costa, and J. M. Lemos, "Diode/magnetic tunnel junction cell for fully scalable matrix-based biochip," *Appl. Phys. Lett.*, vol. 99, no. 8, p. 08B 307, Apr. 2006.

[7] T. M. Almeida *et al.*, "Characterisation and modelling of a magnetic biosensor," in *Proc. Instrum. Meas. Technol. Conf.*, Sorrento, Italy, 2006, pp. 2007–2012.

[8] J. G. Proakis, *Digital Communications*, 4th ed. New York: McGraw-Hill, 2001, ch. 5.1.2.

[9] P. Stoica, H. Li, and J. Li, "Amplitude estimation of sinusoidal signals: Survey, new results, and an application," *IEEE Trans. Signal Process.*, vol. 48, no. 2, pp. 338–352, Feb. 2000.

[10] D. C. Rife and R. R. Boorstyn, "Single-tone parameter estimation from discrete-time observations," *IEEE Trans. Inf. Theory*, vol. IT-20, no. 5, pp. 591–598, Sep. 1974.

[11] A. V. Oppenheim and R. W. Schafer, *Discrete Time Signal Processing*. Englewood Cliffs, NJ: Prentice–Hall, 1999.

[12] S. Haykin, *Adaptive Filter Theory*. Englewood Cliffs, NJ: Prentice–Hall, 1996.

Paulo A. C. Lopes received the Ph.D. degree in electrical and computer engineering from Instituto Superior Técnico, Technical University of Lisbon, Lisbon, Portugal, in 2004.

He is currently an Auxiliary Professor with the Department of Electrical and Computer Engineering and a Researcher with the SIPS Research Group, Instituto de Engenharia de Sistemas e Computadores-Investigação e Desenvolvimento (INESC-ID), Lisbon. His main research interests include digital signal processing for acoustics, telecommunications, biomedical applications, and bioinformatics.

José Germano received the graduate degree in electrical and computer engineering and the M.Sc. degree in 2004 and 2006, respectively, from Instituto Superior Técnico, Technical University of Lisbon, Lisbon, Portugal, where he is currently working toward the Ph.D. degree. His doctoral study focuses on the improvement of a data acquisition and processing platform for DNA recognition using a magnetoresistive biochip.

His research interests include bioelectronics/biomedical instrumentation, implantable and wearable electronics, and processor microarchitectures.

Teresa Mendes de Almeida received the Diploma, M.Sc., and Ph.D. degrees in electrical and computer engineering from Instituto Superior Técnico (IST), Technical University of Lisbon, Lisbon, Portugal, in 1988, 1994, and 2005, respectively.

She is currently a Professor with the Department of Electrical and Computers Engineering, IST, and a Researcher with the Instituto de Engenharia de Sistemas e Computadores-Investigação e Desenvolvimento (INESC-ID), Lisbon. Her research interests include analog and digital phase-locked loops, DSP algorithms, and system modeling.

Leonel Augusto Sousa (M'01–SM'03) received the Ph.D. degree in electrical and computer engineering from Instituto Superior Técnico (IST), Technical University of Lisbon, Lisbon, Portugal, in 1996.

He is currently a Member of the Department of Electrical and Computer Engineering, IST, and a Senior Researcher with Instituto de Engenharia de Sistemas e Computadores-Investigação e Desenvolvimento (INESC-ID), Lisbon. His research interests include computer architectures, parallel and distributed computing, and VLSI architectures for multimedia and biomedical systems.

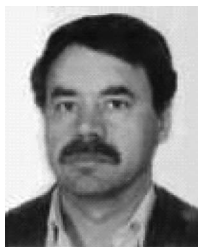

Moisés S. Piedade received the Ph.D. degree in electrical and computer engineering from Instituto Superior Técnico (IST), Technical University of Lisbon, Lisbon, Portugal, in 1983.

He is currently a Professor with the Department of Electrical and Computer Engineering and the Leader of the SIPS Research Group, Instituto de Engenharia de Sistemas e Computadores-Investigação e Desenvolvimento (INESC-ID), Lisbon. His research interests include electronic systems, signal-acquisition and processing systems, and circuits and systems for biomedical applications.

Filipe Arroyo Cardoso received the Diploma degree in physics engineering from Instituto Superior Técnico (IST), Technical University of Lisbon, Lisbon, Portugal, where he is currently working toward the Ph.D. degree.

He is also with Instituto de Engenharia de Sistemas e Computadores Microsistemas & Nanotecnologias (INESC-MN), Lisbon, where he is working on magnetoresistive biochips.

H. A. Ferreira received the Diploma degree in physics engineering from Instituto Superior Técnico, Technical University of Lisbon, Lisbon, Portugal, where he is currently working toward the Ph.D. degree.

He is currently with Instituto de Engenharia de Sistemas e Computadores Microsistemas & Nanotecnologias (INESC-MN), Lisbon, where he is working on magnetoresistive biochips.

Paulo P. Freitas is currently a Full Professor of physics with Instituto Superior Técnico, Lisbon, Portugal, and the Director of the Instituto de Engenharia de Sistemas e Computadores Microsistemas & Nanotecnologias, Lisbon. His current research interests include MRAMS, read heads for ultrahigh-density recording, magnetoresistive biochips, and sensors for biomedical applications.